frontiers | Frontiers in Physics

TYPE Brief Research Report
PUBLISHED 19 August 2022
DOI 10.3389/fphy.2022.770536

OPEN ACCESS

EDITED BY
Steen Grüner Hanson,
Technical University of Denmark,
Denmark

REVIEWED BY
Xinzhong Li,
Henan University of Science and Technology, China
Arindam Dasgupta,
University of Central Florida,
United States

*CORRESPONDENCE
Víctor Martínez-Calzada,
vmartinez@upmh.edu.mx

SPECIALTY SECTION
This article was submitted to Optics and Photonics,
a section of the journal
Frontiers in Physics

RECEIVED 04 September 2021
ACCEPTED 05 July 2022
PUBLISHED 19 August 2022

CITATION
Saldaña-Heredia A, Martínez-Calzada V, Del Villar-Ramírez VU and Rodríguez-Torres A (2022), Optical measurement of an impact reaction in a modeled wing.
Front. Phys. 10:770536.
doi: 10.3389/fphy.2022.770536

Optical measurement of an impact reaction in a modeled wing

Alonso Saldaña-Heredia, Víctor Martínez-Calzada*, Víctor Uriel Del Villar-Ramírez and Adriana Rodríguez-Torres

Universidad Politécnica Metropolitana de Hidalgo, Tolcayuca, Mexico

In this research, an impact reaction which was provoked far from its origins was studied. A metal box filled with sand was used to emulate a rigid body in which a steel bar was embedded; these conditions simulated the fuselage and wing, respectively, and the impact was applied to the rigid body and the measurement to the bar. For this, an optical technique was used to measure the relative displacement of the steel bar, and the measurements are obtained by applying digital image correlation; 2D images were obtained from the speckles generated as a reflection of the beam on the material. The results were studied through the modified Gauss–Newton analytical approach obtaining a maximum standard error deviation of 0.144 from the experimental results.

KEYWORDS

laser speckle, digital image correlation, analytical approach, Gauss-Newton method, error

1 Introduction

Non-invasive tests are widely used in the aeronautic industry, mainly for maintenance purposes, examples of which are visual inspection, microscopy, radiography, and penetrating dyes, among others [1]. Optical tests have been used as a non-invasive technique for measurement purposes, such as flow direction [2], particle image velocimetry [3], and Doppler anemometry [4], among others. In this article, we used an optical technique that helps to evaluate the displacement field on a surface, which could be the fuselage; this technique helps to understand the interaction between an external impact and the surface of a rigid body.

For this technique, we used a laser and two physical principles: propagation and reflection; Snell's law establishes that the reflection of light will occur at the same angle of incidence [5], and there is a special case when light falls on a rough surface, which is why a speckle pattern is generated [6]. Here we study the free propagation of light through the air and the interaction with the surface of interest. Since the reflection is a speckled pattern, we decided to study it using an image matching technique: digital image correlation. Correlation is a well-developed technique used since Kuglin and Hines analytically demonstrated that displacement information was found within images [7]; this technique is widely used in different mechanical measurements [8, 9]. Also, in-plane displacement measurements were applied to understand the response of external forces

through numerical approximation and modeling a reaction [10, 11], to measure vibrations [12], among others.

In this research, a soft impact induced on a rigid body is studied. Such testings were developed using low-strength projectiles impacting different materials [13]. Abrete studied and developed an analytical model of aircraft-induced soft impacts such as raindrops, hail, and bird collision [14]. Aircraft impacts have been studied through numerical models using Lagrangian formulations and finite element coupling different methodologies [15]. Experimental studies have been carried out using strain gauges to measure the local strain in the impacted area [16]. Composite materials have been studied in the interaction of soft impacts using numerical efficiency and prediction [17]. Reza demonstrated the importance of the orientation of a bird using the hydrodynamics of soft particles [18]. Kashfuddoja et al. used correlation to evaluate the elastic properties of a carbon fiber panel [19].

This article was written to study and understand the quantitative and qualitative displacements in an idealized wing. It is well known that both optical measurement techniques and dynamic systems theory are not new and have been applied in many fields. Using these two techniques as an attempt to model the impact reaction in the idealized wing is challenging for us. Let us clarify this. The formulation proposed here can link real parameters with the simple model found, in this case, the weight of the box filled with sand, length's bar, etc. In real airplanes, the fuselage, wings, and their interaction exist and interact; however, analytically or even numerically, the linkage of both structures generates severe problems in the huge system of equations formed. This is due to the diversity of interacting physical and mechanical properties and the size of both structures. For this reason, we looked for and found a way to solve this problem. The displacements found experimentally and theoretically are close to each other and are adequately accurate. In addition to this, we consider that this study can be useful for readers. Finally, the simple formulation could be considered useful information for designers.

2 Methodology

2.1 Optical measurement

In this research, we used a laser as a source to measure the displacements caused on a surface, and we selected an optical system as it is one of the most typical to develop a non-invasive technique [20]. One of the properties of the laser relevant to this study is the intensity since the beam used has a Gaussian distribution [21], which can be written as follows:

$$I(r) = I_0 e^{-\frac{r^2}{\omega_0^2}} \tag{1}$$

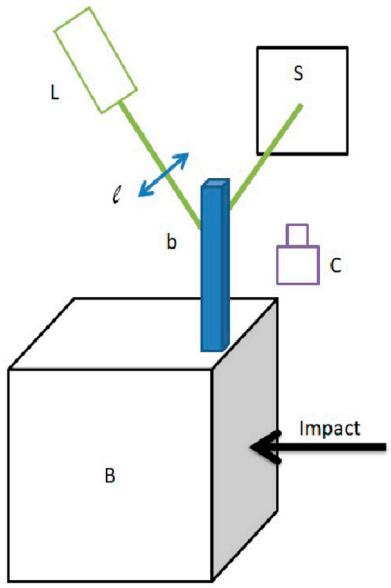

FIGURE 1
Experimental setup, relative displacement measurement of an impact far from its origins.

where I_0 and ω_0 are the initial intensity and the beam waist at $z = 0$, respectively; and I depends on the distance r according to a polar transformation $r = (x^2 + y^2)^{1/2}$ [22]. The intensity of the beam hits a rough material, and when this happens, the reflected intensity results in the interference of scattered components that form a granular pattern known as a speckle pattern [6]. When this physical phenomenon occurs, the intensity changes to

$$P_{(I)} = \frac{1}{4\pi\sigma^2} e^{-\frac{I}{2\sigma^2}} \tag{2}$$

which is known as the probability density function of intensity $P_{(I)}$, where σ is the average intensity of the speckle in the field. It has a very large number of random variables, thus, the central limit theorem is followed [23], as real and imaginary parts of the field are asymptotically Gaussian.

2.2 Metrology system

When the laser hits the surface and is reflected back, the speckles are digitized as 2D images, and thus, an image procedure is followed. Digital image correlation is a well-known procedure, and it is considered an optical technique applied to image data; it comprises capturing consecutive images with a digital camera, which has been used for stress, displacement, and vibration measurements, among others [24–27]. The displacement field (D_f) is obtained through the correlation between images, where two 2D images are needed: A and B; A is used as reference and B is the deformed image. This process is followed by

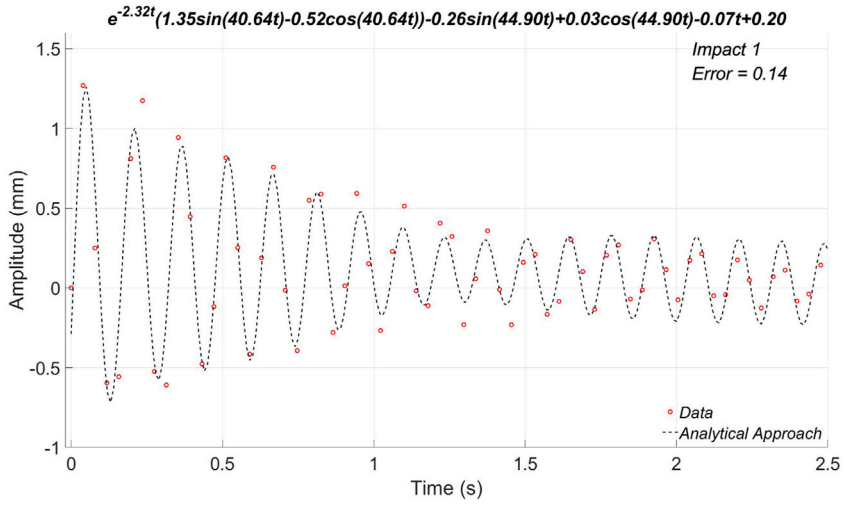

FIGURE 2
Test 1, optical characterization (symbols) and analytical approach (dotted line).

$$D_f = \frac{Re(C_c)}{s_1^2 s_2^2 M} \tag{3}$$

where C_c is the mathematical correlation which is carried out according to [7–11, 24, 27]. Normalization is performed, where M is the image size, and s_1 and s_2 are the standard deviation of the images[11, 27].

2.3 Theoretical analysis

We have simulated harmonic motion with an impact generated by a pendulum. Such motion can be modeled as a damped oscillator, which describes the forced damped motion in the impact direction. Then, the general motion could be described as

$$m\frac{d^2x}{dt^2} + c\frac{dx}{dt} + kx = f(t) \tag{4}$$

where m, c, and k are the mass of the object, the damping coefficient, and the spring constant, respectively. The external force $f(t)$ was proposed as a linear combination of harmonic and linear functions. Hence, we can say that a function that fits (4) looks like

$$x(t) = e^{At}(B\sin(Ct) + D\cos(Ct)) + E\sin(Ft) + G\cos(Ft) + Ht + I \tag{5}$$

where the capital letters are constants. The terms multiplied by the exponential function correspond to the homogeneous solution and the other four terms to the particular solution of (4). Hence, it is possible to apply the modified Gauss–Newton method for fitting the measured values with a non-linear regression function (5) by least squares [28]. Assuming the relation

$$y_i = x(t_i, A, B, \cdots\cdots, I) + e_i \tag{6}$$

where y_i is the measured values, $x(t_i, A, B, \cdots\cdots, I)$ the nonlinear function of the parameters (A, B, ……, I), and e_i an error. The nonlinear model can be linearized using a Taylor series around the parameters and curtailed after the first derivative, that is,

$$x(t_i)_{j+1} = x(t_i)_j + \frac{\partial x(t_i)_j}{\partial A}\Delta A + \frac{\partial x(t_i)_j}{\partial B}\Delta B + \cdots\cdots + \frac{\partial x(t_i)_j}{\partial I}\Delta I \tag{7}$$

Clearly, parameters (A, B, ……, I) in the argument were omitted. j is an initial value for the new estimate $j + 1$. $\Delta(*) = (*)_{j+1} - (*)_j$. Hence, the model is now linearized with respect to the parameters. The substitution of Eq. 7 into Eq. 6 yields

$$y_i - x(t_i)_j = +\frac{\partial x(t_i)_j}{\partial A}\Delta A + \frac{\partial x(t_i)_j}{\partial B}\Delta B + \cdots\cdots + \frac{\partial x(t_i)_j}{\partial I}\Delta I + e_i \tag{8}$$

Using matrix notation, the last equation is rewritten as

$$\Phi = Z_j\Theta + \Sigma \tag{9}$$

where Z_j is a matrix with the partial derivatives of function at the initial value j. Vector Φ contains the difference between data and function values, vector Θ represents parameter values, and Σ the errors, that is,

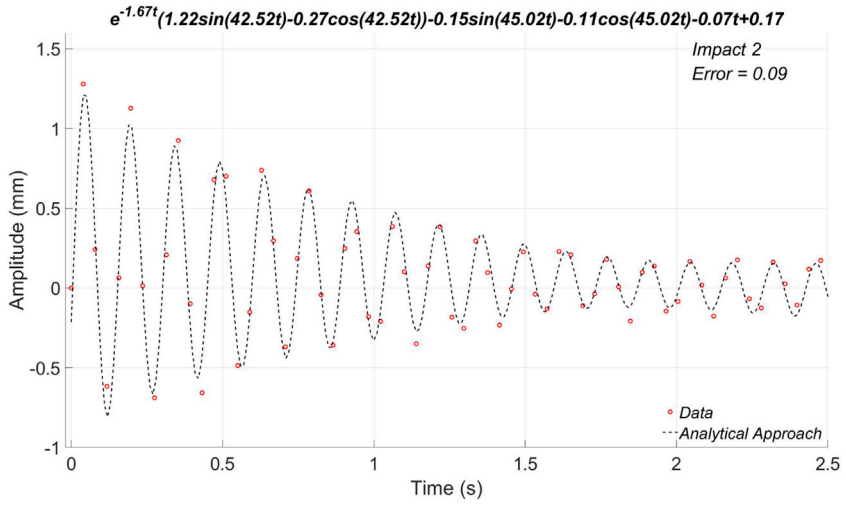

FIGURE 3
Test 2, optical characterization (symbols) and analytical approach (dotted line).

$$Z_j = \begin{bmatrix} \frac{\partial x(t_1)_j}{\partial A} & \frac{\partial x(t_1)_j}{\partial B} & \cdots\cdots & \frac{\partial x(t_1)_j}{\partial I} \\ \frac{\partial x(t_2)_j}{\partial A} & \frac{\partial x(t_2)_j}{\partial B} & \cdots\cdots & \frac{\partial x(t_2)_j}{\partial I} \\ \vdots & \vdots & \ddots & \vdots \\ \frac{\partial x(t_n)_j}{\partial A} & \frac{\partial x(t_n)_j}{\partial B} & \cdots\cdots & \frac{\partial x(t_n)_j}{\partial I} \end{bmatrix}; \quad (10)$$

$$\Phi = \begin{bmatrix} y_1 - x(t_1) \\ y_2 - x(t_2) \\ \vdots \\ y_n - x(t_n) \end{bmatrix}; \qquad \Theta = \begin{bmatrix} \Delta A \\ \Delta B \\ \vdots \\ \Delta I \end{bmatrix}$$

where n is the number of data. After applying the least square method to Eq. 9, we obtain

$$Z_j^T Z_j \Theta = Z_j^T \Phi \quad (11)$$

Once (11) is solved for Θ, the sum of residuals can be calculated as

$$\Gamma(\alpha) = \sum_i^n \left[y_i - x(t_i, \Theta_0 + \alpha\Theta) \right]^2 \quad (12)$$

where Θ_0 is the initial estimate parameter vector, and will have a minimum at [28]:

$$\alpha_{min} = \frac{1}{2} + \frac{1}{4}\left[\frac{\Gamma(0) - \Gamma(1)}{\Gamma(1) - 2\Gamma\left(\frac{1}{2}\right) + \Gamma(0)} \right] \quad (13)$$

In this study, the standard error of the estimate was calculated as

$$Error = \sqrt{\frac{\Gamma(\alpha_{min})}{n-9}} \quad (14)$$

3 Experimental set-up and data processing

A section of the fuselage as a rigid body is modeled through a box (B) with dimensions of 40 × 40 × 40 cm; it was made from galvanized smooth sheet caliber 12 [29], filled at 70% with G 0/3 sand [30] reaching a total mass of 84 kg; this was used to measure the interaction of a collision by means of impacting one of its sides, where the collisions were induced using a 0.575 kg mass; all impacts were done exactly on the mid-point of the transversal area. A square bar (b) with 0.81 cm^2 of the transversal area was embedded into the sand, the total height of this bar was 1 m and the displacement measurements were done at 60 cm. The output of a diode-pumped solid-state laser (L), with a wavelength of λ = 532 nm and power of 220 mW [31] was placed 21 cm far from the bar's surface, and the laser beam propagates through a converging lens (ℓ) with a focal length of f = 7 cm which is placed 13 cm away from (B) to focus the beam of light on a specific area. Subsequently, the scattering generated is reflected in a screen (S), which is placed in front of the box at 50 cm; it is assumed a rigid body (B) is completely still at time t = 0, followed by a collision in the perpendicular face, as shown in Figure 1. While this action is taking place, the speckles generated are recorded with a video camera (C) which is placed in front of the screen, slightly off from the propagation axis.

The camera used in this research can record 240 fps with 1080 × 1080. To depict the video, free software was used [32] that

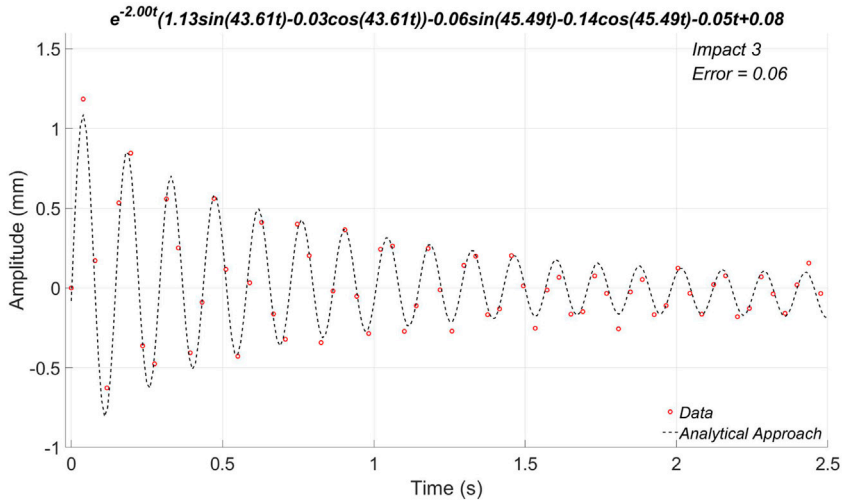

FIGURE 4
Test 3, optical characterization (symbols) and analytical approach (dotted line).

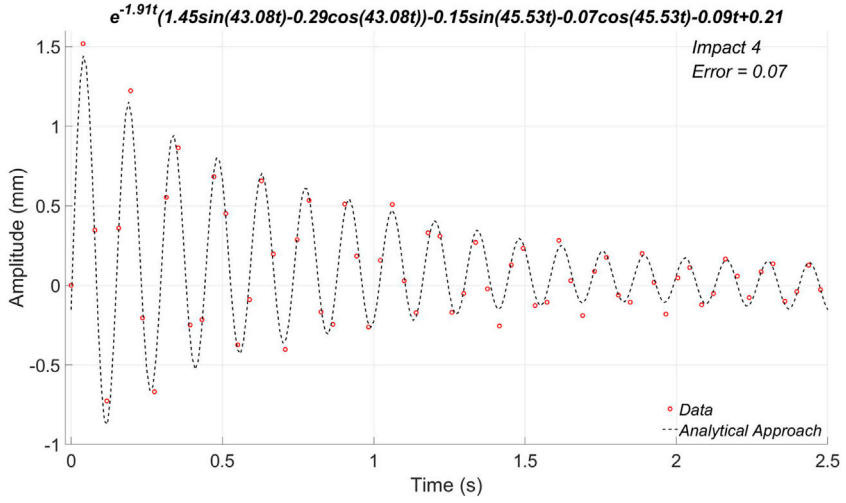

FIGURE 5
Test 4, optical characterization (symbols) and analytical approach (dotted line).

enables all the possible frames. Thus, a code was written in Octave® to perform digital image correlation by following Eqs 5, 6. Those equations gave us a matrix-type result; thus, we define logically the maximum amplitude point, which is part of the intensity field I in Eq. 2, and it is related to the real and imaginary part of the complex amplitude of each speckle [23]. As this is an iterative process, from the second to the n image, those peak amplitudes are plotted as scalar values measured in millimeters according to [10, 11].

4 Results and discussion

In this section, the data were recorded experimentally and the analytical approach is compared. The sampling time in all cases is 2.5 s, and during this period of time, 79 measurements were taken. Data were plotted with symbols while analytical approaches are shown in dotted lines. Clearly, the data show that our experimental model oscillates rapidly, as a damped mass-spring system. The first test is shown in Figure 2. At a

TABLE 1 Characterization of impacts according to the damped mass-spring system.

Impact	Constants			Deviation
	m (kg)	c ($N\frac{s}{m}$)	k ($\frac{N}{m}$)	
1	0.026	0.118	42.308	0.144
2	0.024	0.084	43.002	0.087
3	0.024	0.096	45.575	0.063
4	0.023	0.087	42.428	0.065

glance, it is the worst analytical approach, most data show a gap between them and the methodical approach. However, the qualitative motion is totally reproduced by the proposed model. The mass, damping coefficient, and spring constant of an equivalent damped mass-spring system are 0.026 kg, 0.118 $N\frac{s}{m}$, and 42.308 $\frac{N}{m}$, respectively.

The second test is shown in Figure 3. As can be seen, the analytical approach is closer to the data; in fact, there are just a few points that our approach could not reach. According to this result, the analytical approach corresponds to the optical measurement, exhibiting the motion of the damped mass-spring system. In this case, the equivalent mass, damping coefficient, and spring constant are 0.024 kg, 0.084 $N\frac{s}{m}$, and 43.002 $\frac{N}{m}$, respectively. The best approach was found in the third test, as shown in Figure 4. It is evident that data and the analytical solution are consistent almost everywhere. Once again, the damped motion is clearly reproduced. The equivalent mass, damping coefficient, and spring constant found were 0.024 kg, 0.096 $N\frac{s}{m}$, and 45.757 $\frac{N}{m}$, respectively.

Finally, Figure 5 shows the fourth test, showing that the analytical approach proposed reflects the phenomena quantitative and qualitative. The equivalent mass, damping coefficient, and spring constant are 0.023 kg, 0.087 $N\frac{s}{m}$, and 42.428 $\frac{N}{m}$, respectively. The Table 1 summarizes the results of the tests done. It can be seen how all values keep in the same range, outstanding reproducibility. Mean values for mass, damping coefficient, and spring constant are 0.02425 kg, 0.09625 $N\frac{s}{m}$, and 43.32825 $\frac{N}{m}$, respectively.

5 Conclusion

In this study, an idealization of an impact reaction to a wing was characterized using a laser system coupled with an image-matching procedure. To do that, we proposed the classical model of a damped mass-spring system with linear and harmonic excitation. Measured data were fitted applying the modified Gauss–Newton method with the solution of the mentioned system. In most cases, results show that our analytical approach reproduced quantitative and qualitative phenomena.

Data availability statement

The raw data supporting the conclusion of this article will be made available by the authors, without undue reservation.

Author contributions

All authors listed have made a substantial, direct, and intellectual contribution to the work and approved it for publication.

Acknowledgments

VD-R would like to thank CONACYT for the grant, No. 334455. This work was developed by authors under project PRODEP No. 511-6/220-8515.

Conflict of interest

The authors declare that the research was conducted in the absence of any commercial or financial relationships that could be construed as a potential conflict of interest.

Publisher's note

All claims expressed in this article are solely those of the authors and do not necessarily represent those of their affiliated organizations, or those of the publisher, the editors, and the reviewers. Any product that may be evaluated in this article, or claim that may be made by its manufacturer, is not guaranteed or endorsed by the publisher.

References

1. da Silva RR, Germano X, de Pauda. *Nondestructive inspection reliability: State of the art" in nondestructive testing methods and new applications*. London: IntechOpen (2012). p. 3–23. Chapter 1,.

2. Jebraieli Jolodar A, Akbarnejad MM, Taghizadeh M, Marvast MA. Laser-based flow measurement in performance assessment of FCC atomizer. *Chem Eng J* (2005) 108:109–15. doi:10.1016/j.cej.2005.01.009

3. Raffel M, *Particle Image Velocimetry: A practical guide*, 255. Switzerland: Springer (1998). eBook ISBN: 978-3-662-03637-2.

4. Puharic M, Ristic S, Kutin M, Adamovic Z. Laser Doppler anemometry in hydrodynamic testing. *J Russ Laser Res* (2007) 28:619–28. doi:10.1007/s10946-007-0047-y

5. BahaaSaleh EA, Teich MC. *Fundamentals of Photonics*. United States of America: John Wiley and Sons (1991).

6. Goodman JW. Some fundamental properties of speckle. *J Opt Soc Am* (1976) 66:1145. doi:10.1364/josa.66.001145

7. Kuglin CD, Hines DC. The phase correlation image alignment method. *Proc Int'l Conf Cybernetics Soc* (1975) 163–5.

8. Pradille C, Bellet M, Chastel Y. A Laser speckle method for measuring displacement field. Application to resistance heating tensile test on steel. *Appl Mech Mater* (2010) 24:135–40. doi:10.4028/www.scientific.net/amm.24-25.135

9. Calloch S, Hild F, Marco Y. Digital image correlation used to analyze the multiaxial behavior of rubber-like materials. *Eur J Mech - A/Solids* (2001) 20: 169–87. doi:10.1016/s0997-7538(00)01135-9

10. Saldaña-Heredia A. In-plane displacement for analytical strain determination. *J Mater Sci Eng* (2019) 8510:1–6. doi:10.4172/2169-0022.1000510

11. Saldaña-Heredia A, Mathew J. Characterization of biosurfactant produced by the endophyte Burkholderia sp. WYAT7 and evaluation of its antibacterial and antibiofilm potentials. *J Biotechnol* (2020) 22:1–10. doi:10.1016/j.jbiotec.2020.03.005

12. Baberniss T, Eason T, Spottswood S. High-speed 3D digital image correlation measurement of long-duration random vibration; recent advancements and noted limitations. *Proc Int Conf noise vibration Eng* (2012) 86 1403–16. doi:10.1016/j.ymssp.2016.04.014

13. Wilbeck James S. *Impact behavior of low strength projectiles*. Ohio: Wright-Patterson Air Force Base (1977).

14. Abrete S. Soft impacts on aerospace structures. *Prog Aerospace Sci* (2016) 81: 1–17. doi:10.1016/j.paerosci.2015.11.005

15. Langrand B. Assessment of multi-physics FE methods for bird strike modelling- Application to a metallic riveted airframe. *Int J Crashworthiness* (2002) 415–28. doi:10.1533/cras.2002.0227

16. Hanssen AG, Girard Y, Olovsson L, Berstad T, Langseth M. A numerical model for bird strike of aluminium foam- based sandwich panels. *Int J Impact Eng* (2006) 32:1127–44. doi:10.1016/j.ijimpeng.2004.09.004

17. Guimard JM, Heimbs S. *Towards the industrial assessment of bird strike simulations on composite laminate structures, Composites 2011, 3rd ECCOMAS Thematic Conference on the Mechanical Response of Composites*. Hannover: ECCOMAS (2011).

18. Hedayati R, Ziaei-Rad S. Effect of bird geometry and orientation on bird-target impact analysis using SPH method. *Int J Crashworthiness* (2012) 17(4): 445–59. doi:10.1080/13588265.2012.674333

19. Kashfuddoja M., Prasath R. G. R., Ramji M. Study on experimental characterization of carbon fiber reinforced polymer panel using digital image correlation: A sensitivity analysis. *Opt Lasers Eng* (2014) 62:17–30. doi:10.1016/j.optlaseng.2014.04.019

20. Sirohi R. *Introduction to optical metrology*. U.S.A: Taylor & Francis (2016). ISBN 978-1-4822-3611-8.

21. Alda J. *Laser and Gaussian beam propagation and transformation*. New York, NY: Encyclopaedia of optical Engineering (2003).

22. Wood R. *Physical Optics*. 3rd ed. Washington DC: Optical Science of America (1988).

23. Dainty JC. *Laser speckle and related phenomena*. New York: Springer-Verlag Berlin Heidelberg (1975).

24. Sutton MA, *Image correlation for shape, motion and deformation measurements*. New York, NY: Springer US (2009). p. 322.

25. Hyoung-Suk C, Cheung JH, Kim SH, Ahn JH. Structural dynamic displacement vision system using digital image processing. *NDT E Int* (2011) 44:597–608. doi:10.1016/j.ndteint.2011.06.003

26. Chen F. Overview of three-dimmensional shape measurement using optical methods. *Opt Eng* (2000) 389:10–22. doi:10.1117/1.602438

27. Frike-Begemann T. Optical Mearument of deformation fields and surface processes with digital speckle correlation. Phd Thesis (2002).

28. Hartley HO. The modified Gauss-Newton method for the fitting of non-linear regression functions by least squares. *Technometrics* (1961) 3(2):269–80. doi:10.1080/00401706.1961.10489945

29. Mipsa. Página No encontrada (2021). Available from: https://www.mipsa.com.mx/productos/acero/laminas-y-placas/lamina-galvanizada-lisa/Galvanized sheet.

30. G 0/3 sand. Tabla de densidad de los materiales G 0/3 sand (2021). Available from: http://www.aridsgarcia.com/es/la-oficina-virtual/tabla-de-densidad-de-los-materiales G 0/3 sand.

31. Laserglow Technologies. *LCS-0532 low-cost DPSS laser system laserglow Part Number: C53200XSX , laser product datasheet generated on*. Toronto: Laserglow Technologies (2015).

32. JPG Converter. Windows video to JPG converter (2021). free software Available from: https://free-video-to-jpg-converter.uptodown.com/windows Video to JPG converter.